J Mater Sci (2010) 45:6556–6561
DOI 10.1007/s10853-010-4744-5

The upconversion luminescence properties of the Yb^{3+}–Ho^{3+} system in nanocrystalline Y_2O_2S

Yao Fu · Wanghe Cao · Yong Peng · Xixian Luo · Mingming Xing

Received: 30 September 2009 / Accepted: 28 June 2010 / Published online: 9 July 2010

Abstract Near-spherical Y_2O_2S:Yb^{3+},Ho^{3+} nanocrystals (NCs) with an average particle size of 40 nm were synthesized by the coprecipitation method followed by a solid–gas sulfuration technique. The effects of the Ho^{3+} ion doping concentration on the upconversion luminescence (UCL) property of the NCs was studied through the UCL spectra. Results show that the UCL intensity of Y_2O_2S:Yb^{3+},Ho^{3+} NCs markedly changes with Ho^{3+} ion concentration, and that the Ho^{3+} ion concentration quench is observed at 0.25 mol%. This value is only half as much as that in micron Y_2O_2S prepared by a solid state reaction, which can be attributed to the distinct diffusion mechanism of activator ions in the coprecipitation process. In addition, strong red emissions can be observed in Y_2O_2S:Yb^{3+},Ho^{3+} NCs throughout all Ho^{3+} doping concentrations used. However, the Ho^{3+} in micron Y_2O_2S usually exhibits weak red UCL. Infrared spectra confirm that this result is related to the large vibrational quanta produced by OH^- and CO_3^{2-} groups adsorbed onto the surface of NCs. These large vibrational quanta can remarkably increase the probability of $^5S_2$–$^5F_5$ and $^5I_6$–$^5I_7$ multiphonon relaxation, leading to the enhancement of red emissions arising from $^5F_5 \rightarrow {}^5I_8$ transitions. The UCL mechanism of the Yb^{3+}–Ho^{3+} system in nano- and microsized Y_2O_2S is also discussed.

Y. Fu (✉) · W. Cao · Y. Peng · X. Luo · M. Xing
Department of Physics, Institute of Optoelectronic Technology, Dalian Maritime University, Dalian 116026, Liaoning, People's Republic of China
e-mail: fuyaozn@126.com

Introduction

For decades, nanosized materials have attracted much attention because of their unique and improved optical, electrical, and structural properties compared with conventional bulk materials. Since upconversion luminescence (UCL) was first observed in nanosized Y_2O_3:Er^{3+} by Capobianco et al. [1], UCL from near-infrared (NIR) to visible light in nanocrystals (NCs) has elicited increasing interest because of their wide potential applications in various fields, such as infrared detection, molecule recognition, and three-dimensional displays [2–4]. In recent years, the intense demand for biological fluorescence labels with higher luminescent efficiencies and stabilities have resulted in the widespread application of nanocrystalline upconversion phosphors in the field of biomedicine [5–8].

UCL efficiency depends mainly on the host materials. However, biomedical research requires that the host materials not only possess high luminescence efficiency and excellent chemical stability, but also security and innocuity. Y_2O_2S has been reported as one of the most efficient upconversion hosts because of its advantages, which include a low phonon energy, low symmetry, favorable chemical stability, and nontoxicity; thus, it has attracted considerable attention [9–11]. Currently, studies on nanocrystalline Y_2O_2S UCL materials focus mainly on the Yb^{3+}, Er^{3+} co-doped system [9, 10], and studies on Yb^{3+}, Ho^{3+} co-doped Y_2O_2S NCs are thus far rare. Our previous study demonstrated that the UCL efficiency of the Y_2O_2S:Yb^{3+},Ho^{3+} system is higher than that of Y_2O_2S:Yb^{3+},Er^{3+} [12], suggesting that Y_2O_2S:Yb^{3+},Ho^{3+} NCs have the potential to be applied as biological fluorescence labels with high sensitivity. Unfortunately, although Hirai et al. [10] and Xing et al. [11] successfully synthesized Y_2O_2S:Yb^{3+},Ho^{3+} NCs by liquid membrane

emulsion and homogeneous precipitation methods, respectively, neither of them studied the UCL mechanism of the Yb^{3+}–Ho^{3+} system in detail.

In this paper, Yb^{3+}, Ho^{3+} co-doped Y_2O_2S NCs were prepared by a simple coprecipitation method followed by a solid–gas sulfuration technique, and the special UCL properties and transition mechanism of the Yb^{3+}–Ho^{3+} system in Y_2O_2S NCs were studied extensively.

Experimental section

The Y_2O_2S:Yb^{3+},Ho^{3+} NCs were synthesized by the coprecipitation method followed by a solid–gas sulfuration technique. First, $Y(NO_3)_3{\cdot}5H_2O$, $Ho(NO_3)_3{\cdot}5H_2O$, and $Yb(NO_3)_3{\cdot}5H_2O$ were weighed to stoichiometric ratios and dissolved in 100 mL of distilled water to form aqueous 0.1 M rare earth-nitrate solutions. The rare earth doping concentrations were 6 mol% for the Yb^{3+} ion and 0.1, 0.25, 0.5, 0.75, and 1.0 mol% for the Ho^{3+} ion. A 0.1 M Na_2CO_3 aqueous solution and PEG4000 were then selected as the precipitating agent and surfactant, respectively. To prepare the Y_2O_3:Yb^{3+},Ho^{3+} precursor, the aqueous nitrate solution was added to 150 mL of the 0.1 M Na_2CO_3 solution containing 0.15 g PEG4000 under vigorous stirring. Stirring was continued for 30 min. The resultant precipitates were separated centrifugally at 3000 r/min, and washed twice with distilled water and absolute alcohol. Finally, the obtained precipitates were dried at 60 °C for 12 h and calcined at 600 °C for 1 h to produce the Y_2O_3:Yb^{3+},Ho^{3+} white powders.

The sulfuration of oxides was performed via a solid–gas reaction. The white powders produced were placed into a quartz tube and calcined at 700 and 800 °C. During the calcination, sulfur powders were heated at 400 °C to produce sulfur vapor, which was brought into the tube by an N_2 gas flow for reaction with the Y_2O_3 powder. After the reaction was maintained for 1 h, calcination was terminated and only the N_2 gas flow was supplied. When the samples had been cooled to room temperature, off-white Y_2O_2S:Yb^{3+},Ho^{3+} NCs doped with different Ho^{3+} contents were obtained.

A Shimadzu X-ray diffractometer-6000 using Cu Kα radiation was employed to analyze the crystal size and phase of the samples. The tube voltage used was 40 kV, the tube electric current was 30 mA, and the step velocity was 4°/min. The morphology of the samples was determined by transmission electron microscopy (TEM, Tecnai G^2 20), and the infrared spectrum was obtained using the potassium bromide technique on a Fourier transform infrared spectrometer (Magna 2IRTM 550, USA) in the wavenumber range of 4000–400 cm^{-1}. A Hitachi F-4500 fluorescence spectrophotometer equipped with a 980 nm laser diode was used to obtain the UCL spectra of the samples; the emission slit was 1.0 nm and the excitation powder was 117 mW. For intensity emission comparisons, all UCL spectra were corrected using a xenon lamp as reference. Dark spectra obtained under the same conditions were also subtracted from all UCL spectra. However, the emission spectra were not corrected for the wavelength dependence of the detection system sensitivity and the refractive index of air (vacuum correction).

Results and discussion

Figure 1 presents the XRD spectra of the Y_2O_3:6%Yb^{3+}, 0.25%Ho^{3+} precursor material and the samples sulfurized at different temperatures. The Y_2O_3 precursor obtained crystallizes well and shows a pure cubic phase structure (JCPDS Card No. 74-1828). The considerably broadened diffraction peaks indicate that nanocrystalline Y_2O_3 particles were obtained. When the precursor is sulfurized at 700 °C for 1 h, the intensities of Y_2O_3 diffraction peaks decrease gradually, and some weak diffraction peaks for hexagonal Y_2O_2S structure emerge (JCPDS Card No. 24-1424). After the sulfurized temperature is increased to 800 °C, all diffraction peaks of Y_2O_3 disappear, and only strong Y_2O_2S diffraction peaks remain. This result shows that a temperature higher than 800 °C is beneficial for obtaining pure Y_2O_2S NCs. However, considering that higher temperatures may result in grain growth and particle aggregation, the sulfuration temperature used in this experiment was defined to be 800 °C. According to the Scherrer Formula: $D = \frac{K\lambda}{\beta \cos\theta}$ (where D is the crystal size of the particle, λ is the radiation wavelength of Cu Kα (0.154 nm), and β and θ are the half peak breadth and

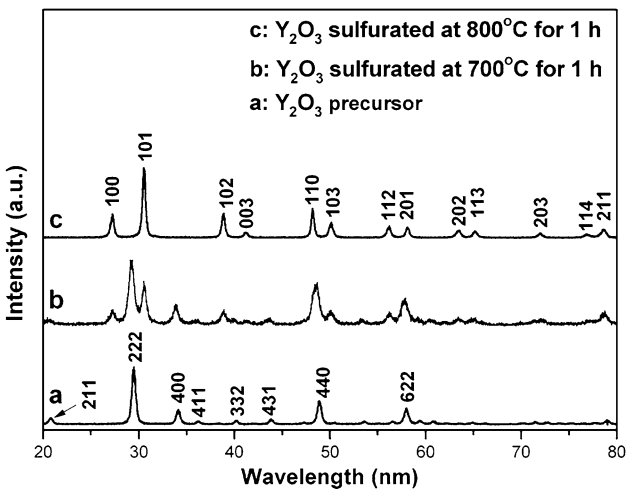

Fig. 1 XRD spectra of Y_2O_3:6%Yb^{3+},0.25%Ho^{3+} precursor and the samples sulfurized at different temperatures

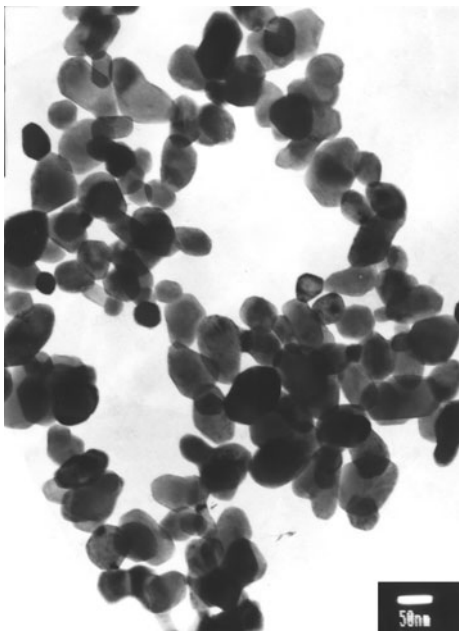

Fig. 2 The TEM image of the Y_2O_2S:6%Yb^{3+},0.25%Ho^{3+} NCs sulfurized at 800 °C

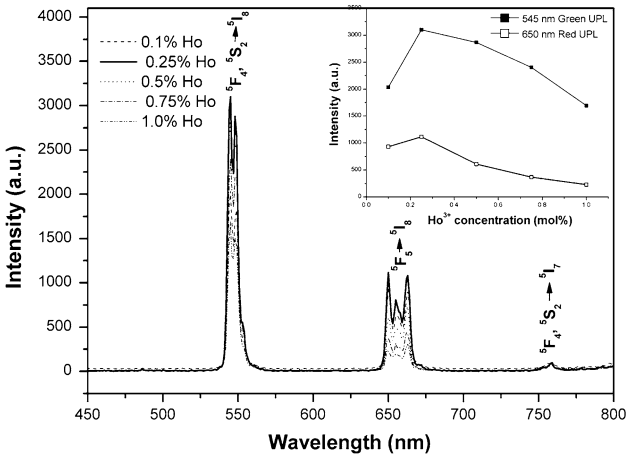

Fig. 3 The UCL spectra of Y_2O_2S:Yb^{3+},Ho^{3+} NCs doped with different concentrations of Ho^{3+} ion (Yb^{3+} content = 6 mol%) excited at 980 nm LD. *Inset*: The plots of green and red UCL intensities versus the Ho^{3+} concentrations

Bragg diffraction angle of the diffraction peak, respectively), the mean crystal size of the Y_2O_2S NCs sulfurized at 800 °C is 22.33 nm. Figure 2 shows the TEM image of Y_2O_2S:6%Yb^{3+},0.25%Ho^{3+} NCs sulfurized at 800 °C. The crystals grow relatively well and exhibit a near-spherical shape. The gain size of the sample averages 40 nm and distributes in the range of 25–50 nm. These results are slightly larger than those obtained from XRD measurements, and can be attributed to the slight aggregation of the primary crystals.

To study the effects of Ho^{3+} ion content on the UCL properties of Y_2O_2S:Yb^{3+},Ho^{3+} NCs, the UCL spectra of Y_2O_2S:Yb^{3+},Ho^{3+} NCs doped with different concentrations of Ho^{3+} ions (Yb^{3+} ion content = 6 mol%) excited at 980 nm LD were obtained, as shown in Fig. 3. The inset in the figure shows the plots of green and red UCL intensities versus the Ho^{3+} ion concentrations used. Note that the peak positions of Ho^{3+} characteristic emissions in Y_2O_2S NCs are consistent with those in bulk Y_2O_2S [12]. The strong green emissions located at 545 and 548 nm arise from $^5F_4$, $^5S_2 \rightarrow {}^5I_8$ transitions. The red emissions observed between 650 and 663 nm correspond to the $^5F_5 \rightarrow {}^5I_8$ transition. The weak NIR emissions located around 759 nm are assigned to $^5F_4$, $^5S_2 \rightarrow {}^5I_7$ transitions.

Figure 3 shows that the variation of Ho^{3+} ion concentrations does not affect the peak positions of Ho^{3+} characteristic emissions. Remarkable influence on the green and red UCL intensities, however, is found. The green UCL intensity improves considerably with increasing Ho^{3+} concentration, whereas the red UCL intensity exhibits weak enhancement. Both intensities attain maximum levels at an Ho^{3+} content of 0.25 mol%. When the Ho^{3+} content is greater than 0.25 mol%, concentration quenching takes place, and the UCL intensities of the green and red emissions begin to gradually decrease. According to the UCL measurement results, the optimal doping concentration of Ho^{3+} ions for green UCL in Y_2O_2S NCs is 0.25 mol%. This value is only half as much as that in micron Y_2O_2S (0.5 mol%) prepared by solid reaction processes [12], and can be ascribed to the distinct diffusion mechanism of activator ions in the coprecipitation process.

During the coprecipitation process, activator ions uniformly distribute into the precursor material produced by the precipitation reaction. While crystallization caused by calcination occurs, activator ions can directly occupy adjacent Y^{3+} lattices, so that the loss of activator ions is very limited. For the solid reaction, however, activator ions have to diffuse gradually from the surface to the interior of the particles. To accelerate this diffusion, some fusing agent is required to form a mass of grain boundary phases between particles and cause the activator ions to diffuse rapidly into the crystal lattices by a grain boundary diffusion mechanism [13]. According to the EDAX quantitative analysis results, most of the activator ions exist in these grain boundary phases, and the amount of ions which have been doped into the lattices and can operate on upconversion emission does not exceed half of the total doping concentration. Thus, the doping concentration of the activator in materials prepared by solid reactions is usually much higher than the actual requirement.

The red UCL of Ho^{3+} ions cannot be effectively suppressed in Y_2O_2S NCs throughout all the Ho^{3+} doping concentrations used in this experiment, especially since Ho^{3+} ions in micron Y_2O_2S typically exhibit considerably

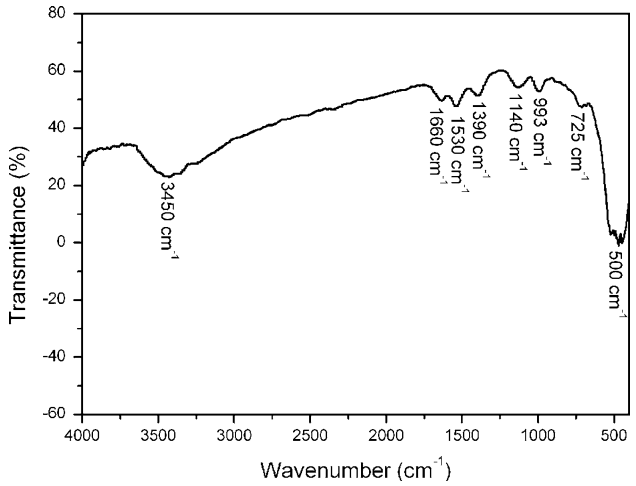

Fig. 4 IR spectrum of Y_2O_2S: 6%Yb^{3+},0.25%Ho^{3+} NCs sulfurized at 800 °C for 1 h

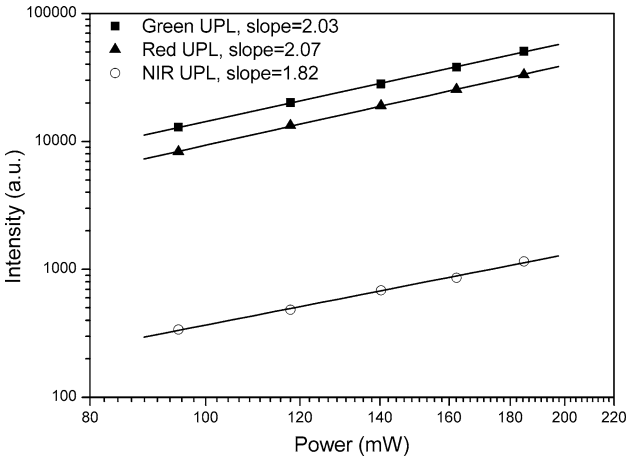

Fig. 5 The integrated intensities of Ho^{3+} ions green, red, NIR emission in Y_2O_2S:6%Yb^{3+},0.25%Ho^{3+} NCs as a function of the pump intensity

weak red UCL [12]. The relatively strong red UCL observed in Y_2O_2S NCs can be ascribed to the high surface activity of the NCs. The amount of NC surface atoms can highly increase with decreases in crystal size. The deficient coordination and high surface energy cause these surface atoms to possess high activity and show weak stability. To decrease surface energy, a sizeable amount of H_2O and CO_2 are absorbed onto the NC particle surfaces to form chemisorbed OH^- and CO_3^{2-}. These findings are demonstrated by the IR spectrum of Y_2O_2S:6%Yb^{3+},0.25%Ho^{3+} NCs sulfurized at 800 °C (Fig. 4). The broad absorption bands around 3450 and 1660 cm^{-1} can be assigned to the stretching and bending vibrations of O–H; the bands around 1530 and 1390 cm^{-1} result from C–O asymmetrical stretching vibrations; the peak that appears at 1140 cm^{-1} can be assigned to C–O symmetric stretching vibrations; the peaks at 993 and 725 cm^{-1} correspond to C–O and O–H deformation vibrations; and the strong peak at $\sim$ 500 cm^{-1} can be assigned to the vibrations of Y–O and Y–S. These large vibrational quanta (3450–1140 cm^{-1}) can considerably influence the transition mechanism of the Yb^{3+}–Ho^{3+} system in Y_2O_2S NCs. To further understand this mechanism, the UCL intensities of Y_2O_2S:6%Yb^{3+},0.25%Ho^{3+} NCs excited by 980 LD with different powers were measured.

The UCL intensity (I_{UCL}) is proportional to some power n of the incident excitation power (I_P) so that

$$I_{UCL} \propto I_P^n$$

where the superscript $n = 1, 2, 3\ldots$ represents the number of pump photons required to populate the emitting states. The integrated intensities calculated from the area under the green, red, and NIR emissions in Y_2O_2S:6%Yb^{3+}, 0.25%Ho^{3+} NCs as a function of the pump intensity are shown in Fig. 5. The n values are calculated to be 2.03, 2.07, and 1.82 for the green, red, and NIR emission bands, respectively. These indicate that two IR photon absorptions are involved in the emission processes. According to the abovementioned results, the transition mechanism of the Yb^{3+}–Ho^{3+} system in Y_2O_2S NCs can be built (Fig. 6).

Under 980 nm LD excitation, the Ho^{3+} ions in the ground $^5I_8$ state are excited to $^5F_4$, $^5S_2$ states via two successive energy transfers from the Yb^{3+} ions in the $^2F_{5/2}$ state. Transitions from the $^5F_4$, $^5S_2$ states to the $^5I_8$ and $^5I_7$ states then yield green and NIR emissions, respectively. These transition processes are the same as those in micron Y_2O_2S. However, the red UCL observed from 650–663 nm shows a large difference in the transition mechanisms of the system under study and micron Y_2O_2S. The energy gaps (ΔE) of $^5S_2$-$^5F_5$ and $^5I_6$-$^5I_7$ are 2660 and 3220 cm^{-1}, respectively. According to the energy gap law, efficient multiphonon relaxation can take place only when ΔE is equal to or less than 4–5 times the highest energy phonons

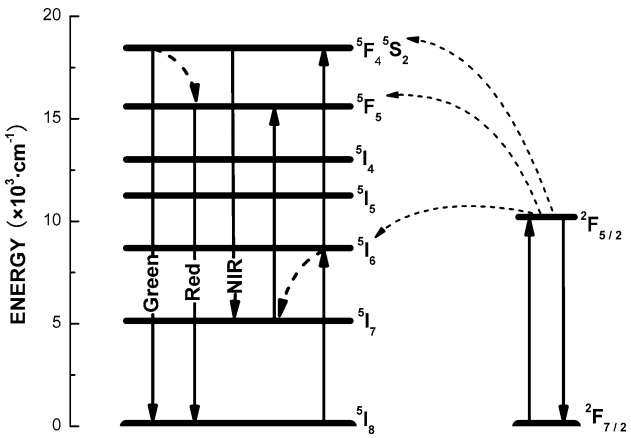

Fig. 6 The transition mechanism of Yb^{3+}–Ho^{3+} system in Y_2O_2S NCs

in the system. For micron Y_2O_2S co-doped with Ho^{3+} and Yb^{3+} ions, its only intrinsic phonon energy (about 520 cm^{-1}) can hardly bridge the large energy difference between the levels mentioned above, and no other phonons are available for its use. Thus, the $^5F_5$ red emission state of Ho^{3+} in micron Y_2O_2S is populated mainly by infrequent $^5F_4/^5S_2 \rightarrow {}^5I_7$ radiative transitions and the subsequent $^5I_7 \rightarrow {}^5F_5$ excited-state absorption process (Route 1). Therefore, only weak red UCL can be observed in micron Y_2O_2S.

For the Y_2O_2S NCs, however, as mentioned previously, the OH^- and CO_3^{2-} groups chemisorbed onto the surface of the NCs can produce large vibrational quanta of 1500 and 3350 cm^{-1}. These quanta can easily bridge the energy gaps of $^5F_4/^5S_2$-$^5F_5$ and $^5I_6$-$^5I_7$, and accordingly increase the probability of $^5F_4/^5S_2 \rightarrow {}^5F_5$ and $^5I_6 \rightarrow {}^5I_7$ multiphonon relaxation. Thus, except for Route 1, the population route of the $^5F_5$ state in the NCs should also include the process of $^5F_4/^5S_2 \rightarrow {}^5F_5$ multiphonon relaxation (Route 2) and the process of $^5I_6 \rightarrow {}^5I_7$ multiphonon relaxation, followed by $^5I_7 \rightarrow {}^5F_5$ excited-state absorption (Route 3). Routes 2 and 3 can increase the population of $^5F_5$ red emission states to a large extent; hence, stronger red emissions can be observed in nanosized Y_2O_2S. Similar phenomena can also be observed in other nanomaterials doped with rare earth metals [3, 14]. Vetrone et al.'s report revealed that vibrations from OH^- and CO_3^{2-} groups can be still observed even after heating NCs to 1000 °C for 65 h [3].

The prepared $Y_2O_2S:Yb^{3+},Ho^{3+}$ NCs exhibit bright green emission in the daytime that is visible to the naked eye at excitation powers as low as 25 mW ($I_G/I_R = 2.53$). Because previous studies on green UCL in NCs focused mainly on the Yb^{3+}, Er^{3+} co-doped system, for purposes of comparison, $Y_2O_2S:Yb^{3+}$, Er^{3+} NCs were also prepared using the procedure described in reference literature [15]. To obtain approximate I_G/I_R values, the doping concentrations of both Yb^{3+} and Er^{3+}ions selected for this paper were 0.5 mol% ($I_G/I_R = 2.09$; the higher the Yb^{3+} or Er^{3+} ion content, the lower the I_G/I_R value is [15]). Figure 7 shows that in equivalent excitation conditions, the relative UCL intensities of $Y_2O_2S:Yb^{3+},Ho^{3+}$ and $Y_2O_2S:Yb^{3+}$, Er^{3+} NCs can be directly evaluated according to their UCL spectra. The green UCL intensities of the Yb^{3+}–Ho^{3+} system are all three times higher than those of the Yb^{3+}-Er^{3+} system throughout all the powers measured (inset, Fig. 7).

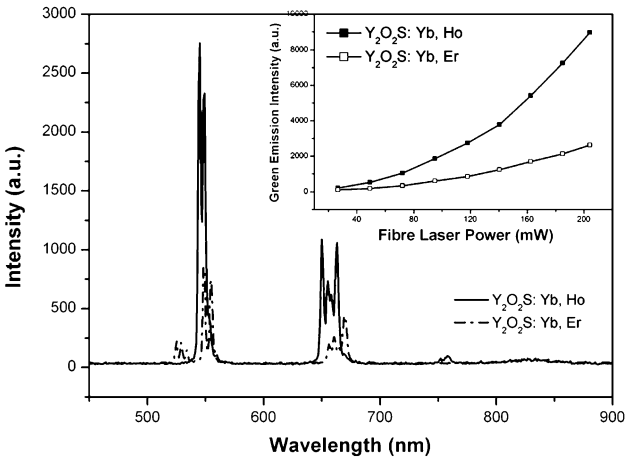

Fig. 7 The comparison of UCL intensities for $Y_2O_2S:Yb^{3+},Ho^{3+}$ and $Y_2O_2S:Yb^{3+}$, Er^{3+} NCs under 980 nm infrared excitation. *Inset*: The plots of green UCL intensities of $Y_2O_2S:Yb^{3+},Ho^{3+}$ and $Y_2O_2S:Yb^{3+}$, Er^{3+} NCs versus the excitation powers

Conclusion

Near-spherical $Y_2O_2S:Yb^{3+},Ho^{3+}$ NCs with hexagonal structure were synthesized using the coprecipitation method followed by a solid–gas sulfuration technique. The crystal size of the NCs average 40 nm and are distributed from 25 to 50 nm. Because the coprecipitation method can ensure the uniform distribution of activator ions in the precursor material, the activator ions can directly occupy the adjacent Y^{3+} lattices during the crystallization process, thereby effectively decreasing the loss of Ho^{3+} ions. Consequently, the optimal doping concentrations of Ho^{3+} ions in Y_2O_2S NCs is 0.25 mol%—only half as much as that in micron Y_2O_2S. The UCL spectra indicate that the Ho^{3+} content can considerably influence the UCL efficiency of Y_2O_2S NCs. The large vibrational quanta produced by OH^- and CO_3^{2-} groups adsorbed onto the surface of the NCs can remarkably increase the probability of $^5S_2$–$^5F_5$ and $^5I_6$–$^5I_7$ multiphonon relaxation. These relaxation processes greatly enhance the population of $^5F_5$ red emission levels, thereby producing stronger red emissions from nanosized Y_2O_2S than from micro Y_2O_2S. These results are of importance in research studies that aim to determine nanosized upconversion biological fluorescence labels with high sensitivity.

Acknowledgements The authors would like to acknowledge the financial support from the National Natural Science Foundation of China (No. 60979003), the Foundation of University Research Program by Liaoning Educational Committee (No. 2009A095), New Century Educational Talents Plan of Chinese Education Ministry (No. NCET-10-0171), and Basic Research Training Foundation of China (No. 2009JC22).

References

1. Capobianco JA, Vetrone F, D'Alesio T, Tessari G, Speghini A (2000) Phys Chem Chem Phys 2(14):3203

2. Wang XF, Xiao SG, Yang XL, Ding JW (2008) J Mater Sci 43(4):1354. doi:10.1007/s10853-007-2266-6
3. Konishi T, Shimizu M, Kameyama Y, Soga K (2007) J Mater Sci Mater Electron 18(S1):183
4. Zako T, Nagata H, Terada N, Sakono M, Soga K, Maeda M (2008) J Mater Sci 43(15):5325. doi:10.1007/s10853-008-2776-x
5. Hampl J, Hall M, Mufti N, Yao YM, MacQueen DB, Wright WH, Cooper DE (2001) Anal Biochem 288(2):176
6. Rijke F, Zijlmans H, Li S, Vail T, Raap AK, Niedbala RS, Tanke HJ (2001) Nat Biotechnol 19(3):273
7. Zijlmans HJMAA, Bonnet J, Burton J, Kardos K, Vail T, Niedbala RS, Tanke HJ (1999) Anal Biochem 267(1):30
8. Tan MQ, Ye ZQ, Wang GL, Yuan JL (2004) Chem Mater 16(12):2494
9. Pires AM, Serra OA, Davolos MR (2004) J Alloys Compd 374 (1–2):181
10. Hirai T, Orikoshi T (2004) J Colloid Interface Sci 273(2):470
11. Xing MM, Cao WH, Pang T, Ling XQ (2009) Solid State Commun 149(23–24):911
12. Luo XX, Cao WH (2007) Mater Lett 61(17):3696
13. Luo XX, Cao WH, Xiao ZG (2006) J Alloys Compd 416 (1–2):250
14. Rosa EDL, Salas P, Desirena H, Angeles C, Rodríguez RA (2005) Appl Phys Lett 87(24):241912
15. Zhong HY, Cao WH (2009) J Funct Mater 40(6):896